Combination Effect of Organics-Modified Montmorillonite with Intumescent Flame Retardants on Thermal Stability and Fire Behavior of Polyethylene Nanocomposites

Guobo Huang,[1] Bingchun Zhu,[2] Haibo Shi[3]

[1]*School of Pharmaceutical and Chemical Engineering, Taizhou University, Linhai, Zhejiang, People's Republic of China*
[2]*Zhejiang Research Institute of Chemical Industry, Hangzhou, Zhejiang, People's Republic of China*
[3]*Applied Biology Department, Zhejiang Pharmaceutical College, Ningbo, Zhejiang, People's Republic of China*

Received 26 May 2010; accepted 21 August 2010
DOI 10.1002/app.33256
Published online 2 March 2011 in Wiley Online Library (wileyonlinelibrary.com).

ABSTRACT: A combination effect was observed between organics-modified montmorillonite (OMMT) and a novel intumescent flame retardant, diphenylmethanamine spirocyclic pentaerythritol bisphosphonate (PSPD), in low-density polyethylene (LDPE) nanocomposites. The results from X-ray diffraction and transmission electron microscopy showed that montmorillonite can achieve better dispersion in LDPE/PSPD blend matrix, and exfoliated LDPE/PSPD/OMMT nanocomposites are formed. Thermal stability and flammability properties were investigated by thermogravimetric analysis and cone calorimeter tests. The combination effect of PSPD and montmorillonite improved thermal stability and reduced significantly the flammability (including heat release rate, total heat release, average mass loss rate, etc.). The peak heat release rate of LDPE/PSPD/OMMT is reduced by about 51% compared with pure LDPE. The morphology and composition of residues generated after cone calorimeter tests were investigated by scanning electron microscopy and X-ray photoelectron spectroscopy. The scanning electron microscopy images showed that the compact and dense intumescent char is formed for LDPE/PSPD/OMMT nanocomposite after combustion. The results of X-ray photoelectron spectroscopy confirmed that the carbon content of the char for LDPE/PSPD/OMMT increases obviously by the combination effect of PSPD and montmorillonite. © 2011 Wiley Periodicals, Inc. J Appl Polym Sci 121: 1285–1291, 2011

Key words: clay; flame retardant; nanocomposites; polyethylene (PE)

INTRODUCTION

Recently, polymer layered silicate nanocomposites (PLSN) have drawn more and more attention because of their unique behaviors. The addition of layered silicates, even at a very lower concentration level (usually less than 5 wt %), into a polymeric matrix can significantly improve polymer properties such as mechanical, thermal, flame-resistant, and flame-barrier properties.[1–12] Previous researches of the flame-retardant properties of PLSN mainly demonstrate a significant decrease in the heat release rate (HRR), a change in the char structure, and a decrease in the mass loss rate during combustion in a cone calorimeter.[13–20] Unfortunately, most of PLSN usually do not extinguish and burn slowly until most of the fuel has been burnt.

To further improve flame-retarding performance of PLSN, flame retardant has been used. As environmentally friendly halogen-free products, intumescent flame retardants (IFRs) are preferably applied in polyolefin materials in place of halogen-containing products because of their advantages of low toxicity and relatively high flame-retarding efficiency.[21–25] The IFR produces a swollen multicellular char layer while burning, which protects the underlying material from the action of the fire and acts as a physical barrier against heat transmission and oxygen diffusion, thus preventing pyrolysis of the materials to volatile combustible materials. However, most commonly used intumescent systems, such as phosphates, pentaerythritol, and melamine, do not have sufficient thermal stability under the processing temperature of polyolefin materials and cannot be incorporated into polymer matrix. In our study, a novel phosphorous–nitrogen-containing IFR, diphenylmethanamine spirocyclic pentaerythritol bisphosphonate (PSPD) was synthesized and applied to polyethylene as a flame retardant.

Combination effects of layered silicates and flame retardant have been already reported for polypropylene,[16,26,27] ethylene vinyl acetate,[28,29] polyurethane,[30,31] and acrylonitrile–butadiene–styrene resin.[32,33] Combinations of montmorillonite and flame retardant are necessary to obtain satisfactory performance. The focus

Correspondence to: G. Huang (huangguobo@tzc.eud.cn).

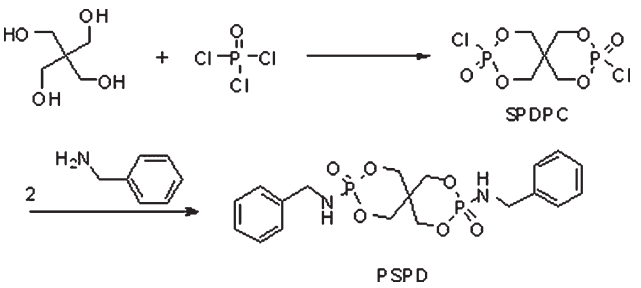

Figure 1 Synthesis of PSPD.

of this work was to study combination effects between phosphorous–nitrogen-containing IFR and layered silicates in low-density polyethylene (LDPE), which was achieved by adding amounts of PSPD and organics-modified montmorillonite (OMMT) during preparation of the nanocomposites. The montmorillonite dispersion was investigated by X-ray diffraction (XRD) and transmission electron microscopy (TEM). The combination effect of PSPD and montmorillonite on thermal stability and flame retardancy was investigated by thermogravimetic analysis (TGA) and cone calorimeter. The char residue after combustion was also examined by scanning electron microscopy (SEM) and X-ray photoelectron spectroscopy (XPS). The results indicated that the combination effect of PSPD and montmorillonite can improve thermal stability and flame retardancy of the nanocomposites.

EXPERIMENTAL

Materials

Commercial LDPE (LDPE-2426H) was supplied by BASF-YPC Co., Ltd. (Nanjing, China). Pristine sodium montmorillonite (Na-MMT), with a cation exchange capacity about 120 mmol/100 g was mined at Anji, Zhejiang, China, and was supplied by Anji Yu Hong Clay Chemical Co., Ltd. (Zhejiang, China). The OMMT was prepared by ion-exchange of Na-MMT and hexadecyl trimethyl ammonium bromide in aqueous solution. All reagents commercially available were used as received unless otherwise stated. Spirocyclic pentaerythritol bisphosphorate disphosphoryl chloride[34,35] was prepared according to the published procedure.

Synthesis of PSPD

PSPD was prepared by the following steps (Fig. 1): phenylmethanamine (0.2 mol) and triethylamine (0.4 mol) were mixed in a glass flask, and then spirocyclic pentaerythritol bisphosphorate disphosphoryl chloride (0.1 mol) dissolved in acetonitrile was added to the mixture gradually. After reaction for 6 hr at 30°C, the raw product was filtered and purified with ethanol and dried at 80°C. The white solid powder was obtained (yield, 88%; melting point, 210–212°C). ^{1}H-NMR (500 MHz, dimethyl sulfoxide [DMSO], δ): 7.35 ~ 7.22 (m, 10H), 6.00 ~ 5.90 (m, 2H),4.39 ~ 4.17(m, 8H), 4.07 ~ 3.97(m, 4H). ^{13}C-NMR (500 MHz, DMSO, δ): 141.16, 128.88, 127.65, 127.49, 68.17, 44.74, 36.13. High-resolution mass spectrometry (electrospray ionization): $C_{19}H_{24}N_2O_6P_2$ calcd mass 438.1110, found 438.1117.

Preparation of the composites

LDPE, OMMT, and IFR (PSPD) were mixed in a twin-screw extruder with a length/diameter ratio of 32 and a screw diameter of 30 mm. The extruding temperature was 190°C for each sample (Table I). The final pellets of the composites were pressed on a curing machine at 150°C for 8 min to be shaped into 3.0 ± 0.1 mm thick sheets for further measurements.

Characterization and measurement

^{1}H- and ^{13}C-NMR spectra were recorded by a Bruker Avance III (500 MHz) spectrometer in DMSO or deuterated chloroform, using tetramethylsilane as an internal standard. High-resolution mass spectrometry was performed with a Therm LCQ TM Deca XP plus mass spectrometer coupled to a Waters 2695 liquid chromatograph. XRD patterns were obtained in Thermo ARL X'TRA diffractometer using a CuK-α (λ = 0.154 nm) radiation generator. The diffraction patterns were collected within the 2θ range 2–20° using scanning rate of 0.6°/min. TEM samples were cut using a diamond knife and RMC MTXL ultramicrotome. TGA was carried out on a Q600SDT thermogravimetric analyzer. Sample weight is in the range of 13.0 ~ 14.0 mg, respectively. All samples of TGA were measured from 30°C to 600°C at a heating rate of 10°C/min with a continuous nitrogen flow. The flame-retardant characteristics of the composites were tested using cone calorimeter (model ASTME1354-93 and ISQ5660) with heat flux of 35 kW/m^2 using a cone radiator. All samples with the dimensions of 10 cm × 10 cm × 3 mm plates were placed in aluminum foil, and then put in a box with the same dimension in the horizontal direction. The cone data reported here were an average of three replicated measurements. Char residue was examined

TABLE I
Formulations for Flame-Retarded LDPE/OMMT Systems

Sample code	Proportions (g)		
	LDPE	PSPD	OMMT
LDPE	100	0	0
LDPE/OMMT	95	0	5
LDPE/PSPD10	90	10	0
LDPE/PSPD20	80	20	0
LDPE/PSPD/OMM	80	15	5

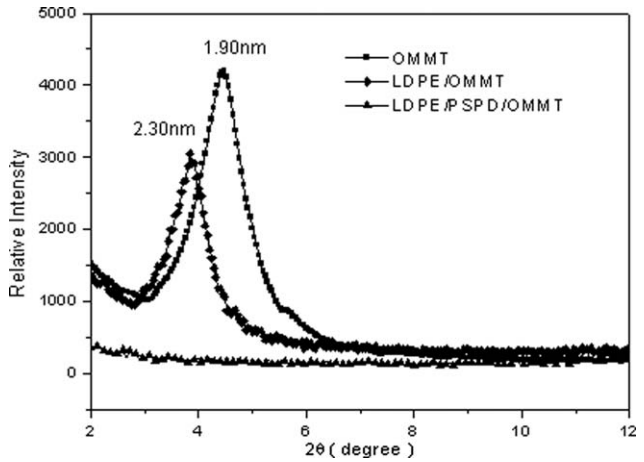

Figure 2 XRD patterns of OMMT, LDPE/OMMT, and LDPE/PSPD/OMMT.

by SEM using Hitachi S-4700(II) scanning electron microscope. XPS data were obtained with an ESCA-Lab220i-XL electron spectrometer from VG Scientific using 300W AlK-α radiation. The base pressure was about 3×10^{-9} mbar. The binding energies were referenced to the C1s line at 284.6 eV from adventitious carbon.

RESULTS AND DISCUSSION

Morphology

Figure 2 shows the XRD patterns of OMMT, LDPE/OMMT, and LDPE/PSPD/OMMT. The basal spacing of the material was calculated from the angular position 2θ of the observed reflection peaks based on the Bragg's law $\lambda = 2d \sin \theta$, where λ is the wavelength of the X-rays and θ is the scattering angle. The (001) reflection of montmorillonite indicated a basal spacing of 1.90 nm. LDPE/OMMT showed a basal spacing of 2.30 nm. The increased spacing indicated that some LDPE molecular chains were intercalated. The characteristic (001) reflection disappeared for LDPE/PSPD/OMMT, which indicated that the clay mineral may be delaminated in the presence of PSPD. PSPD is a low-melting-point organic flame retardant and functions as a plasticizer improving the polymer chain mobility; thus, the LDPE polymer chains are able to intercalate into the layers more easily, and the delamination process of the clay layers will be accomplished more effectively because of existence of PSPD.

To further investigate the clay dispersion in the polymer matrix, TEM analysis was carried out, and the results are shown in Figure 3. TEM micrograph for LDPE/OMMT reveals that the clay mineral layers consisted of multilayered stacks. No serious agglomeration was observed, and a few individual silicate layers were seen, indicating the intercalated structure. In the micrographs of LDPE/PSPD/OMMT, much better dispersion of the montmorillonite and many single clay mineral layers were seen, which indicated that the clay mineral is delaminated and exfoliated LDPE/PSPD/OMMT nanocomposites are formed. This proves that the plasticization of PSPD improves the dispersion of MMT in the polymer matrix. All TEM results further support the XRD data.

Thermal stability

Figure 4 shows the TGA and differential weight loss (DTG) thermograms of PSPD, pure LDPE, LDPE/OMMT, LDPE/PSPD blends, and LDPE/PSPD/OMMT. The TGA and DTG data are summarized in Table II. As the TGA and DTG curves show in Figure 5, the temperature where the weight loss exhibits 5 wt % is defined as the initial decomposition temperature, which is denoted as $T_{initial}$; the temperature at which the degradation rate reaches a maximum is defined as T_{max}.[33,36] PSPD decomposes at 260°C and has a

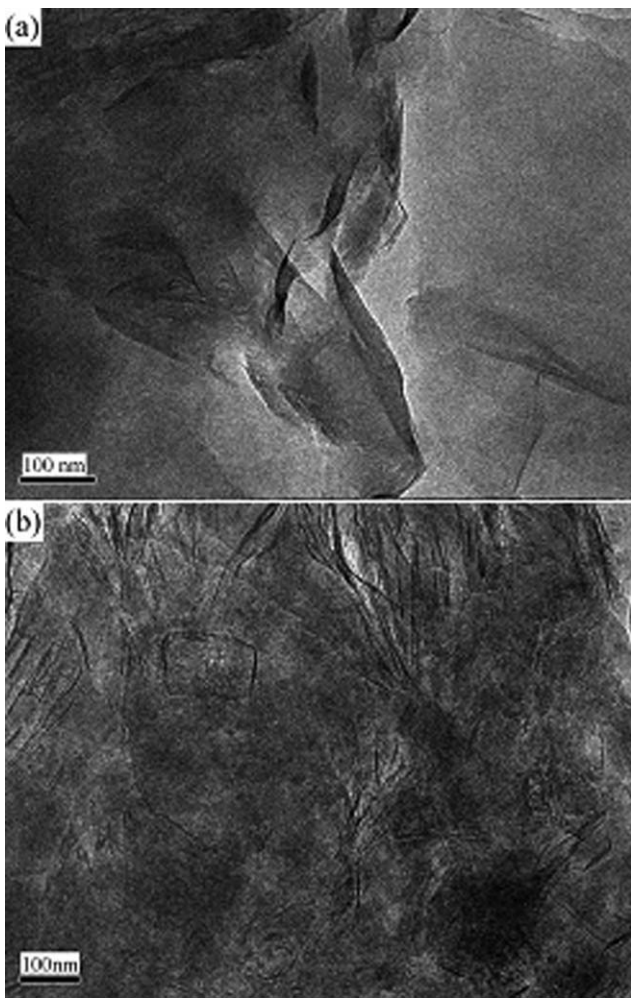

Figure 3 TEM images of (a) LDPE/OMMT and (b) LDPE/PSPD/OMMT.

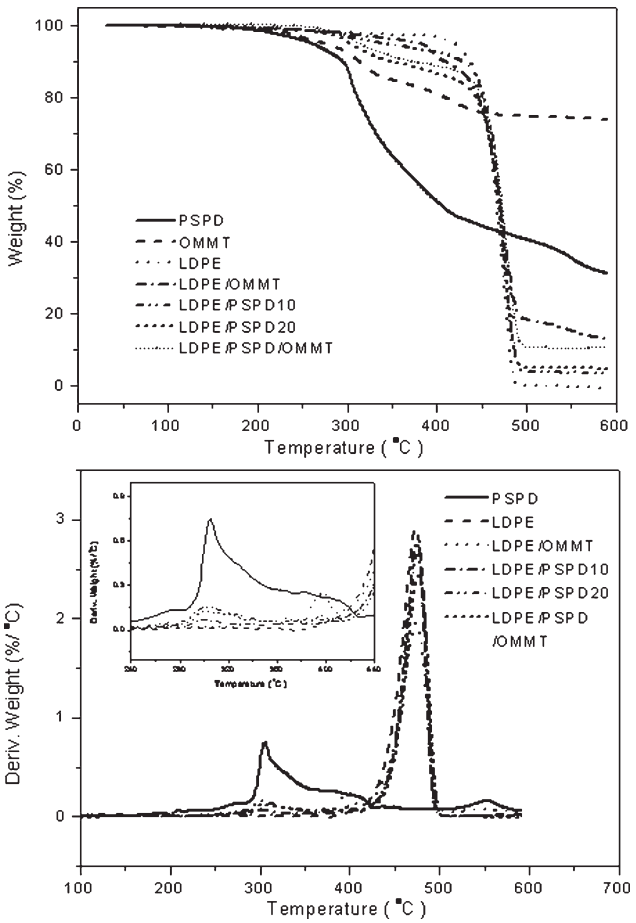

Figure 4 TGA and DTG curves for PSPD, LDPE, LDPE/OMMT, LDPE/PSPD blends, and LDPE/PSPD/OMMT at a heating rate of 10°C/min in N_2.

residue of 31 wt % at 600°C in N_2, indicating the excellent carbonization ability of PSPD. Pure LDPE decomposes at 420°C, leaving negligible char at 600°C. For LDPE/OMMT, a two-steps degradation (380–420°C and 450–500°C, respectively) was found. The first-step degradation is caused by the decomposition of the organic modifier, which results in that $T_{initial}$ of LDPE/OMMT is lower than LDPE. A larger residue showed an enhanced thermal stability

TABLE II
Data of TGA and DTG Thermograms for Various Samples at a Heating Rate of 10°C/min in N_2

Sample	$T_{initial}$ (°C)	Residue at 600°C (wt %)	T_{max} (°C) Stage 1	T_{max} (°C) Stage 2
PDPS	260.5	31	–	301.4
LDPE	420.3	<1	–	481.3
LDPE/OMMT	382.6	4	401.5	482.0
LDPE/PSPD10	342.4	4	307.7	486.6
LDPE/PSPD20	303.2	5	308.4	487.1
LDPE/PSPD/OMMT	313.7	11	310.8	490.6

$T_{initial}$, initial degradation temperature (temperature at 5% weight loss); T_{max}, maximum weight loss temperature.

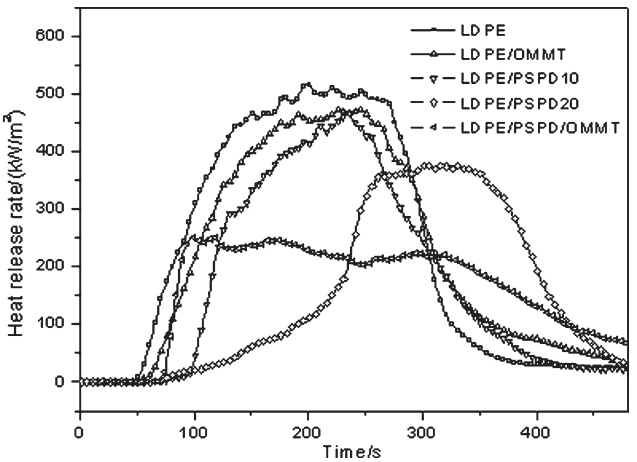

Figure 5 HRR of LDPE, LDPE/OMMT, LDPE/PSPD blends, and LDPE/PSPD/OMMT at 35 kW/m^2.

because of the barrier properties of clay mineral layers. The DTG results showed a lower maximum degradation rate in LDPE/OMMT than that of pure LDPE. For LDPE/PSPD blends, a two-step degradation (250–330°C and 450–500°C, respectively) was found. The first-step degradation is caused by the decomposition of PSPD. $T_{initial}$ of PSPD-containing samples is lower than that of the uncontained one because of earlier degradation of PSPD; however, the maximum mass loss rate at T_{max} of the major degradation step decreases slightly for the PSPD-contained samples, indicating the thermal enhancing effect of PSPD. A significant change in thermal stability was found for LDPE/PSPD/OMMT. The value of T_{max} was significantly improved, almost 3°C higher than LDPE/PSPD20. The final char for LDPE/PSPD/OMMT was 6 wt % higher than that for LDPE/PSPD20. In addition, $T_{initial}$ of LDPE/PSPD/OMMT increases about 10°C compared with the LDPE/PSPD20 blend. Results from TGA and DTG thermograms showed that the combination of OMMT with PSPD can significantly enhance the thermal stability of flame-retarded acrylonitrile–butadiene–styrene systems, especially at the high temperature range and enhance the char formation.

Fire behavior

Figure 5 shows the HRR of LDPE, LDPE/OMMT, LDPE/PSPD10, LDPE/PSPD20, and LDPE/PSPD/OMMT at 35 kW/m^2. The corresponding cone calorimetry data are shown in Table III. Compared with pure LDPE, peak heat release rates (PHRR) and average heat release rate (AHRR) of LDPE/OMMT reduced by 5.7% and 25%, even though total heat release (THR), average specific extinction area (ASEA), and average mass loss rate (AMLR) remain almost same. The time of ignition (t_{ign}) of LDPE/OMMT was 2 sec lower than that of pure LDPE. For

TABLE III
Cone Calorimetry Data for Various Samples at 35 kW/m^2

Term	LDPE	LDPE/OMMT	LDPE/PSPD10	LDPE/PSPD20	LDPE/PSPD/OMMT
t_{ign} (sec)	44 ± 2	41 ± 2	54 ± 1	59 ± 3	56 ± 2
PHRR (kW/m^2)	523 ± 7	493 ± 5	485 ± 4	383 ± 3	253 ± 3
AHRR (kW/m^2)	324 ± 1	243 ± 2	228 ± 2	152 ± 1	140 ± 1
THR (MJ/m^2)	105 ± 1	103 ± 0.9	83 ± 0.5	76 ± 0.3	80 ± 0.5
ASEA (m^2/kg)	407 ± 18	405 ± 15	718 ± 18	722 ± 18	599 ± 14
AMLR (g/sec)	0.079 ± 0.003	0.057 ± 0.002	0.064 ± 0.002	0.045 ± 0.001	0.040 ± 0.001

t_{ign}, time of ignition; PHRR, peak release rate; AHRR, average heat release rate; THR, total heat release; ASEA, average specific extinction area; AMLR, average mass loss rate.

LDPE/PSPD blends, the PHRR, AHRR, and AMLR were reduced significantly with the addition of PSPD. The PHRR was reduced by 7.3% and 26.8% for LDPE/PSPD10 and LDPE/PSPD20 relative to pure LDPE. The THR is reduced by 20.9% and 27.6% for LDPE/PSPD10 and LDPE/PSPD20; the t_{ign} of LDPE/PSPD blends were longer than that of pure LDPE. However, The ASEA of LDPE/PSPD blends were higher than that of pure LDPE. The reason may be because much smoke are produced from the decomposition of PSPD-containing phenyl group. Compared with pure LDPE, the PHRR of LDPE/PSPD/OMMT was reduced by about 51%. For LDPE/PSPD/OMMT, t_{ign} was longer than those of LDPE/OMMT and LDPE/PSPD20. Meanwhile, the values of PHRR, AHRR, THR, and AMLR of LDPE/PSPD/OMMT were lower than those of LDPE/OMMT and LDPE/PSPD20, which indicates that the combination effect of PSPD and OMMT improves the flammability properties of LDPE.

Analysis of the residues' char

Figure 6 shows the digital photos for the residues of LDPE, LDPE/OMMT, LDPE/PSPD20, and LDPE/PSPD/OMMT samples after cone calorimeter tests.

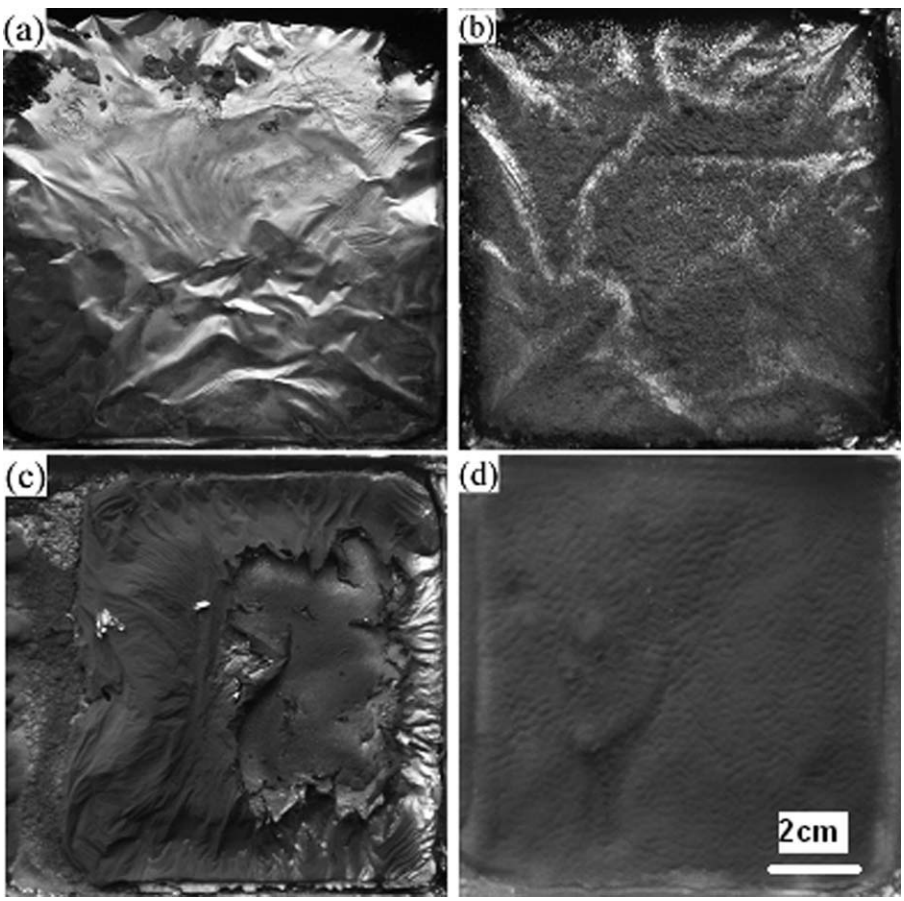

Figure 6 Digital photos of the residues after cone calorimeter testing: (a) LDPE, (b) LDPE/OMMT, (c) LDPE/PSPD20, and (d) LDPE/PSPD/OMMT.

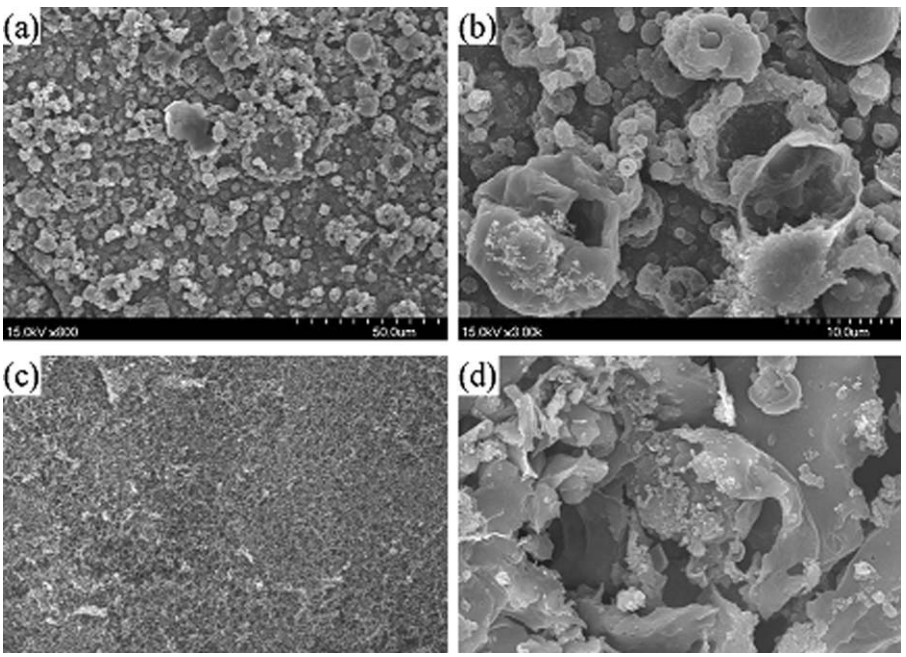

Figure 7 SEM morphology of the char samples obtained from LDPE/PSPD20 outer surface (a) and inner surface (b) and LDPE/PSPD/OMMT outer surface (c) and inner surface (d).

The digital photos demonstrated that the pure LDPE was almost burnt out. For LDPE/OMMT sample, char is thin and discrete. LDPE/PSPD20 sample has swollen chars with some small holes. For LDPE/PSPD/OMMT sample, more rigid, compact, and uniform char is observed.

The morphologies of the charred layers obtained after cone calorimeter test were examined by SEM as shown in Figure 7. Loosely distributed spherical carbonaceous structures were observed in the outer surface of LDPE/PSPD20 char [Fig. 7(a)]. Figure 7(b) shows the image of inner surface of LDPE/PSPD20 char, which has swollen chars with a lot of small bladders of about 1–5 μm diameter. The outer surface of LDPE/PSPD/OMMT char [Fig. 7(c)] showed a more compact and dense char layer compared with LDPE/PSPD20 blend, which can cut off oxygen from the degraded volatiles more efficiently. Figure 7(d) shows that many clay mineral layers were dispersed uniformly on the swollen inner surface of LDPE/PSPD/OMMT char, which can form protective shields and inhibit the transmission of heat and heat diffusion when exposed to flame or heat source. These are other evidences to prove the combination effect of IFR PSPD and montmorillonite during swollen char formation.

Figure 8 presents the XPS spectra of LDPE/PSPD20 and LDPE/PSPD/OMMT after cone calorimeter testing. The elemental compositions of all the studied spectra are summarized in Table IV. As shown in Figure 8 and Table IV, the IFR PSPD took part in the dehydration of the carbonific compounds, which results in that phosphorus still remains in the

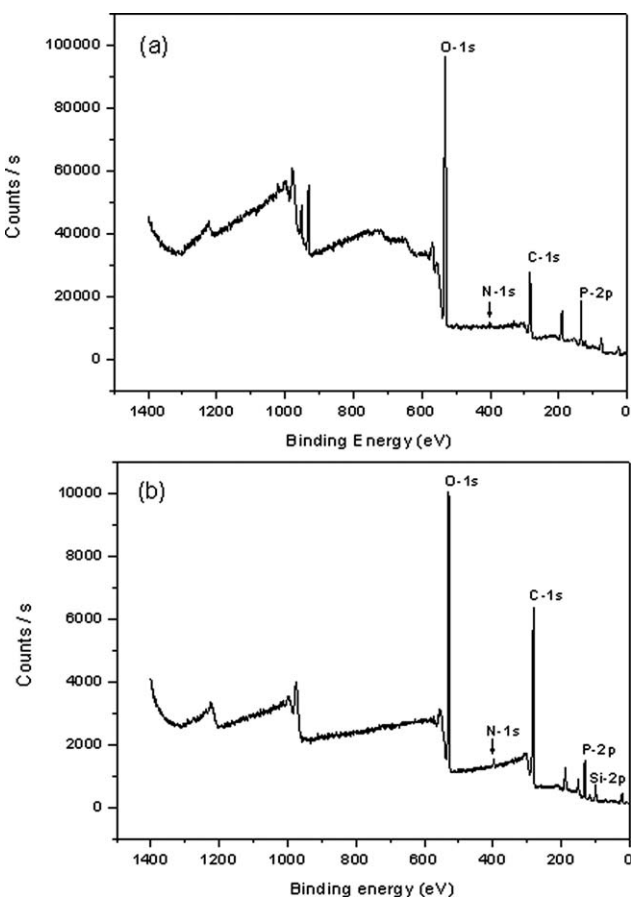

Figure 8 XPS spectra of (a) LDPE/PSPD20 and (b) LDPE/PSPD/OMMT after cone calorimeter testing.

TABLE IV
XPS Data for LDPE/PSPD20 and LDPE/PSPD/OMMT after Cone Calorimeter Testing

Sample	Mass content (%)				
	C	O	P	N	Si
LDPE/PSPD20	28.80 ± 0.34	58.80 ± 0.49	16.91 ± 0.19	0.50 ± 0.03	–
LDPE/PSPD/OMMT	43.42 ± 0.42	39.28 ± 0.36	11.34 ± 0.14	0.47 ± 0.03	5.49 ± 0.09

chars. The blowing agent decomposes to yield gaseous products, which causes the char to swell and the element of nitrogen to greatly decrease. The carbon content of the char for LDPE/PSPD/OMMT was higher than that of LDPE/PSPD20, indicating that the combination effect of PSPD and montmorillonite improve flame retardancy of the nanocomposites.

CONCLUSIONS

LDPE/PSPD/OMMT nanocomposites were prepared by melt blending of LDPE with IFR PSPD and OMMT. The results from XRD and TEM showed that montmorillonite can achieve better dispersion in LDPE/PSPD blend matrix and exfoliated LDPE/PSPD/OMMT nanocomposites are formed, which is attributed to the plasticization of PSPD. A combination effect was found between PSPD and montmorillonite, which improved thermal stability and flame retardancy. Compared with pure LDPE, the PHRR of LDPE/PSPD/OMMT is reduced by about 51%. The SEM images confirmed that the compact and dense intumescent char is formed for LDPE/PSPD/OMMT nanocomposite after combustion. From the analysis of XPS, a conclusion could be deduced that the carbon content of the char for LDPE/PSPD/OMMT increases obviously by the combination effect of IFR PSPD and montmorillonite.

References

1. Paul, D. R.; Robeson, L. M. Polymer 2008, 49, 3187.
2. Rao, Y.-Q.; Pochan, J. M. Macromolecules 2007, 40, 290.
3. Liu, S.-P.; Huang, I.-J.; Chang, K.-C.; Yeh, J.-M. J Appl Polym Sci 2010, 115, 288.
4. Zanetti, M.; Bracco, P.; Costa, L. Polym Degrad Stab 2004, 85, 657.
5. Bertini, F.; Canetti, M.; Audisio, G.; Costa, G.; Falqui, L. Polym Degrad Stab 2006, 91, 600.
6. Yang, L.; Hu, Y.; Lu, H.-D.; Song, L. J Appl Polym Sci 2006, 99, 3275.
7. Lakshmi, M. S.; Narmadha, B.; Reddy, B. S. R. Polym Degrad Stab 2008, 93, 201.
8. Shi, Y.-R.; Kashiwagi, T.; Walters, R. N.; Gilman, J. W.; Lyon, R. E.; Sogah, D. Y. Polymer 2009, 50, 3478.
9. Kaya, E.; Tanoğlu, M.; Okur, S. J Appl Polym Sci 2008, 109, 834.
10. Latta, G.; Lineberry, Q.; Ozao, R.; Zhao, H.-Y.; Pan, W.-P. J Mater Sci 2008, 43, 2555.
11. Beyer, G. Fire Mater 2001, 25, 193.
12. Tyan, H.-L.; Leu, C.-M.; Wei, K.-H. Chem Mater 2001, 13, 222.
13. Janowska, G.; Rybinski, P.; Jantas, R. J Therm Anal Cal 2007, 87, 511.
14. Chuang, T.-H.; Guo, W.-J.; Cheng, K.-C.; Chen, S.-W.; Wang, H.-T.; Yen, Y.-Y. J Polym Res 2004, 11, 169.
15. Song, R.-J.; Wang, Z.; Meng, X.-Y.; Zhang, B.-Y.; Tang, T. J Appl Polym Sci 2007, 106, 3488.
16. Tang, Y.; Hu, Y.; Wang, S.-F.; Gui, Z.; Chen, Z.-Y.; Fan W.-C. Polym Int 2003, 52, 1396.
17. Gilman, J.-W.; Jackson, C.-L.; Morgan, A.-B.; Harris, R., Jr. Chem Mater 2000, 12, 1866.
18. Berta, M.; Lindsay, C.; Pans, G.; Camino, G. Polym Degrad Stab 2006, 91, 1179.
19. Bourbigot, S.; Devaux, E.; Xavier, F. Polym Degrad Stab 2002, 75, 397.
20. Zhang, H.-F.; Wang, Y.-Q.; Wu, Y.-P.; Zhang, L.-Q.; Yang, J. J Appl Polym Sci 2005, 97, 844.
21. Xie, F.; Wang, Y.-Z.; Yang, B.; Liu, Y. Macromol Mater Eng 2006, 291, 247.
22. Ma, Z.-L.; Gao, J.-G.; Niu, H.-J.; Ding, H.-T.; Zhang, J. J Appl Polym Sci 2002, 85, 257.
23. Ma, Z.-L.; Gao, J.-G.; Bai, L.-G. J Appl Polym Sci 2004, 92, 1388.
24. Wang, D.-Y.; Cai, X.-X.; Qu, M.-H.; Liu, Y.; Wang, J.-S.; Wang, Y.-Z. Polym Degrad Stab 2008, 93, 2186.
25. Peng, H.-Q.; Zhou, Q.; Wang, D.-Y.; Chen, L.; Wang, Y.-Z. J Ind Eng Chem 2008, 14, 589.
26. Chen, X.-S.; Yu, Z.-Y.; Liu, W.; Zhang, S. Polym Degrad Stab 2009, 94, 1520.
27. Tang, Y.; Hu, Y.; Li, B.-G.; Liu, L.; Wang, Z.-Z.; Chen, Z.-Y.; Fan, W.-C. J Polym Sci Part A: Polym Chem 2004, 42, 6163.
28. Li, B.; Jia, H.; Guan, L.-M.; Bing, B.-C.; Dai, J.-F. J Appl Polym Sci 2009, 114, 3626.
29. Chigwada, G.; Panchatapa, J.; Jiang, D.-D.; Wilkie, C.-A. Polym Degrad Stab 2005, 89, 85.
30. Song, L.; Hu, Y.; Tang, Y.; Zhang, R.; Chen, Z.; Fan, W. Polym Degrad Stab 2005, 87, 111.
31. Modesti, M.; Lorenzetti, A.; Besco, S.; Hrelja, D.; Semenzato, S.; Bertani, R.; Michelin, R.-A. Polym Degrad Stab 2008, 93, 2166.
32. Wang, S.-F.; Hua, Y.; Zong, R.-W.; Tang, Y.; Chen, Z.-Y.; Fan, W.-C. Appl Clay Sci 2004, 25, 49.
33. Ma, H.-Y.; Tong, L.-F.; Xu, Z.-B.; Fang, Z.-P. Appl Clay Sci 2008, 42, 238.
34. Ma, H.-Y.; Tong, L.-F.; Xu, Z.-B.; Fang, Z.-P.; Jin, Y.-M.; Lu, F.-Z. Polym Degrad Stab 2007, 92, 720.
35. Ma, H.-Y.; Tong, L.-F.; Xu, Z.-B.; Fang, Z.-P. Adv Funct Mater 2008, 18, 414.
36. Zhao, C.-X.; Liu, Y.; Wang, D.-Y.; Wang, D.-L.; Wang, Y.-Z. Polym Degrad Stab 2008, 93, 1323.